Features of Silicon Photo Multipliers: Precision Measurements of Noise, Cross-Talk, Afterpulsing, Detection Efficiency

Paolo Finocchiaro, Alfio Pappalardo, Luigi Cosentino, Massimiliano Belluso, Sergio Billotta, Giovanni Bonanno, and Salvatore Di Mauro

***Abstract*—Solid state single photon detectors are an emerging issue, with applications in the wide field of sensors and transducers. A new kind of device named Silicon Photomultiplier (SiPM) shows timing and charge resolution features that in some respect could even replace traditional photomultiplier tubes. In this paper we illustrate a complete method for the evaluation of gain, dark noise, afterpulsing, cross-talk and detection efficiency of SiPM detectors. We show the application of the method by comparing the performance of our newly developed SiPM (produced by ST Microelectronics) with another sensor present on the market (produced by Hamamatsu), and proving that our device is indeed already outstanding.**

***Index Terms*—Afterpulsing, dark noise, gain, photon detection efficiency, quenching resistor, single photon counting, silicon photomultiplier, single photon avalanche photodiode.**

I. Introduction

SOLID state single photon detectors are nowadays an emerging issue, with promising applications in the wide field of sensors and transducers. A new kind of planar semiconductor device has slowly but steadily come out, namely the Silicon Photomultiplier (SiPM), with outstanding features that in some respect could replace traditional photomultiplier tubes. Based on a Geiger-mode avalanche photodiode elementary cell sensitive to single photons, it consists of an array of n independent identical microcells whose outputs are connected together. The final output, being the analog superposition of n identical signals, allows in principle to build a perfect photosensor capable of detecting and counting the single photons in a light pulse [1]–[15]. Moreover, due to its compact structure and avalanche working principle, the SiPM is intrinsically a fast device capable of time resolution of the order of 100 ps.

Unfortunately there are several drawbacks, basically deriving from its noise features, which can prevent the straightforward use of SiPM detectors in several applications [15]–[19].

Manuscript received June 22, 2008; revised September 05, 2008. Current version published June 17, 2009.

P. Finocchiaro is with INFN Laboratori Nazionali del Sud, Catania 95125, Italy (e-mail: finocchiaro@infn.lns.infn.it).

A. Pappalardo and L. Cosentino are with INFN Laboratori Nazionali del Sud, Catania 95125, Italy.

M. Belluso, S. Billotta, G. Bonanno, S. Di Mauro are with INAF Osservatorio Astronomico di Catania, 95125, Italy.

Color versions of one or more of the figures in this paper are available online at http://ieeexplore.ieee.org.

Digital Object Identifier 10.1109/TNS.2009.2014308

TABLE I
FEATURES OF THE TESTED SIPM DETECTORS

	SiPM STM 32b9-10x10-A	MPPC Hamamatsu S10362-11-100U
Shape	square	square
N. of cells	10x10	10x10
Active area size	0.5mm x 0.5mm	1.0mm x 1.0mm
Geometrical fill factor	36%	78%
Breakdown voltage	29.5 V	68.6 V
Opto-insulation trench	yes	no

In this paper, we will illustrate a method for the evaluation of gain, dark noise, afterpulsing, cross-talk and detection efficiency of SiPM detectors. At the same time we show how the method is useful to compare the performance of different devices. We do so by comparing our newly developed SiPM, produced by ST Microelectronics [30], with a SiPM produced by Hamamatsu [31], and proving that the device performance is indeed promising.

Both the devices we compared consist of a 10×10 array with common readout, whose basic features are summarized in Table I. Apart from other technological differences between the two devices, the main difference which can heavily affect the overall noise figure, as we will see in the following, is the presence in the STM device of an opto-insulation trench around each elementary cell which prevents stray photons produced in an avalanche from triggering new avalanches in neighbouring cells [6], [16], [26].

II. Charge Response to Light

In order to test the response to light we made use of a pulsed laser system, featuring 1 kHz repetition rate, 40 ps FWHM pulse width, 671 nm wavelength. As a first step we connected our sensors to a digital oscilloscope capable of building the so-called persistence plot. It consists of a 2D histogram of many signal traces, with time along X, voltage along Y, and where the third dimension, represented in different colors (or gray levels), is proportional to the number of occurences.

What one expects in dark conditions is a well populated band, due to random noise and then involving one SiPM cell at a time, plus some tiny occurrence of random coincidences giving rise to signals with double amplitude. In Fig. 1 we show the persistence plot of the dark noise for the STM photosensor. Shown are the intense band due to 1-cell random pulses, and the much less frequent band due to 2-cell pulses. In Fig. 2 we show a typical snapshot of the persistence plot of the STM photosensor

0018-9499/$25.00 © 2009 IEEE

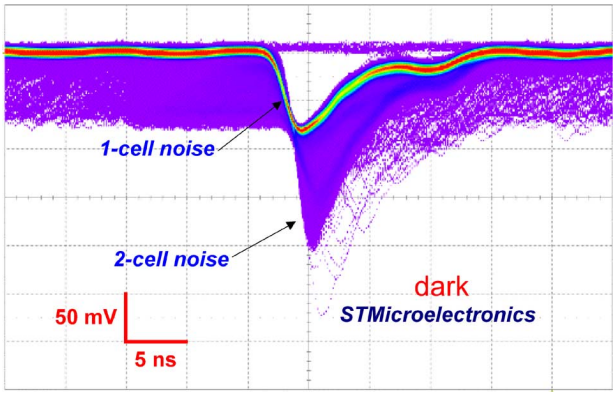

Fig. 1. Snapshot of a persistence plot of the dark noise on a digital scope for the STM photosensor. The total duration of a signal is 10 ns.

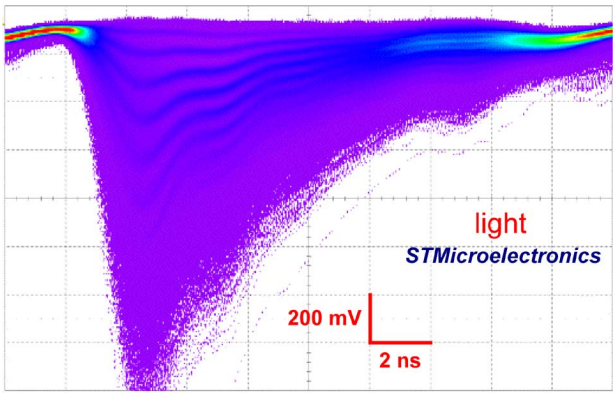

Fig. 2. Snapshot of a persistence plot of laser light signals on a digital scope for the STM photosensor.

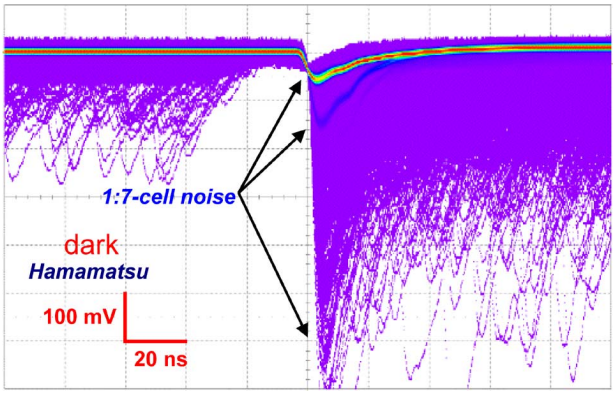

Fig. 3. Snapshot of a persistence plot of the dark noise on a digital scope for the Hamamatsu photosensor. The total duration of a signal is 20 ns.

when illuminated by the laser at low intensity. The detection of discrete numbers of photons is visible in form of well separated darker bands. The corresponding plots for the Hamamatsu sensor are shown in Figs. 3 and 4.

What is immediately evident is that the dark behavior of the two sensors is quite different, whereas the light behavior looks rather similar.

The STM sensor does not show dark pulses with more than two cells involved, and this is a clear indication that its

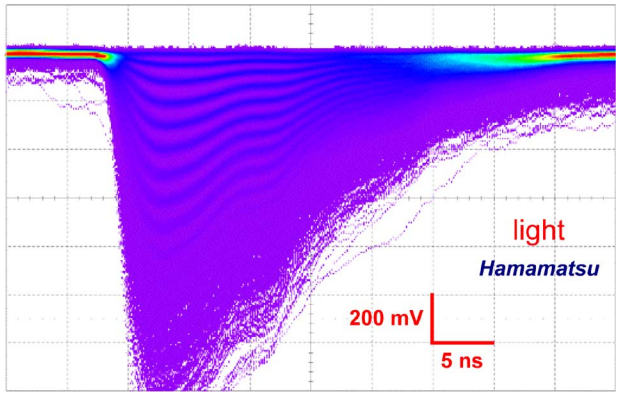

Fig. 4. Snapshot of a persistence plot of laser light signals on a digital scope for the Hamamatsu photosensor.

cross-talk level is low. Due to statistical reasons, there is a small chance that two random counts occur within a given time window ($<10^{-3}$ in 50 ns), whereas the probability of three such counts has to be tiny ($\approx 10^{-5}$ in 50 ns). The Hamamatsu sensor (Fig. 3) shows dark counts with up to seven cells in coincidence, implying a statistically correlated process.

Moreover, the envelope of the untriggered signals before and after the triggered one in Fig. 1 is on the same 1-cell level; this is not the case in Fig. 3, where the higher level after the triggered signal indicates the presence of a considerable amount of afterpulses. In the following chapters we will show how to quantify these indications.

In order to understand the device behavior we collected a series of charge histograms for both devices, under several different conditions of bias voltage and laser intensity. We remark that the laser light was driven to the sensors by means of a fiber placed on top, and that the intensity we quote here is the nominal value set via the laser controller unit. The intensity ranges were suitably chosen in order to scale for the different size (1/4) and geometrical efficiency (0.36/0.78) of the two sensors under test, therefore operating with roughly the same number of impinging photons in the two cases.

The bias voltages were chosen such that they covered the whole useful range for each device, well beyond the breakdown in order to have a reasonable gain but below the values where the noise becomes intolerable. All of the measurements were done at the room temperature of 20°C. In Fig. 5 we show such a histogram for the STM SiPM, whereas Fig. 6 represents the same spectrum for the Hamamatsu device. We tried to fit the experimental data using the following Poisson distribution folded with Gaussian peaks whose variance scales with the order n of the peaks themselves:

$$F(x) = A\frac{dP}{dx} = A \cdot \sum_{n=1}^{\infty} \mathrm{Poisson}(\mu, n) \cdot \frac{1}{\sigma_{\mathrm{tot}}(n)\sqrt{2\pi}} \cdot e^{-\frac{[x-c(n)]^2}{2\sigma_{\mathrm{tot}}^2(n)}} \quad (1)$$

with

$$\sigma_{\mathrm{tot}}^2(n) = \sigma_e^2 + n\sigma_1^2 \quad (2)$$

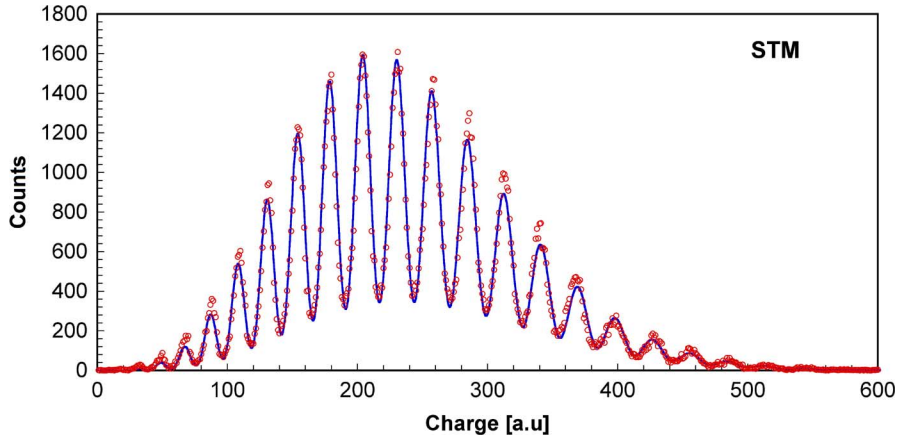

Fig. 5. Charge spectrum of low intensity laser pulses, built using the STM silicon photomultiplier biased at 32.5 V (circles). The continuous line is a fit with the function described in the text.

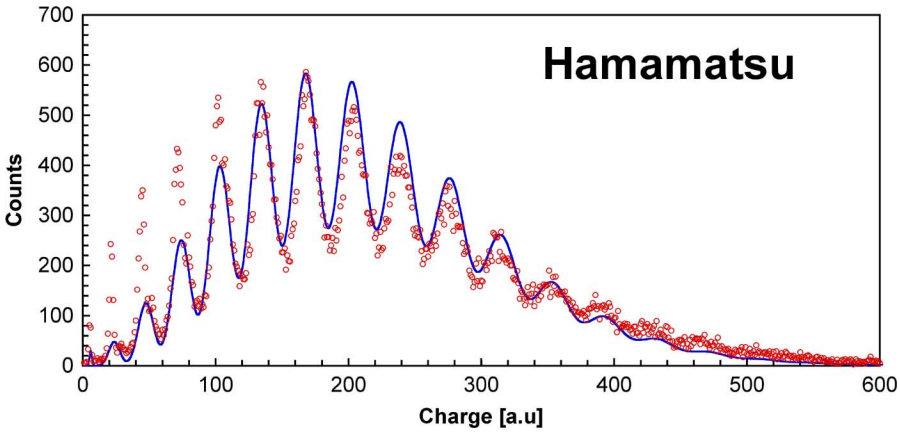

Fig. 6. Charge spectrum of low intensity laser pulses, built using the Hamamatsu silicon photomultiplier biased at 69.7 V (circles). The continuous line is a fit with the function described in the text. Such a fit does not follow reliably the data, especially on the first four peaks. This is an indication of non-poissonian behavior.

A is a normalization constant, equal to the integral of the measured spectrum.

μ is the average value of the Poisson distribution.

$c(n)$ is a stepwise function expressing the coordinate of the centroid of the n peaks. For additional details on the fit see [27], [33].

What we found is that the spectrum in Fig. 5 is reasonably reproduced by the fit. This is not the case with the spectrum in Fig. 6, especially for the first four or five peaks, thus indicating a non-poissonian behavior of the device. This can immediately be interpreted as a direct consequence of the correlated noise (cross-talk and afterpulsing) observed in Fig. 3 for the Hamamatsu sensor.

The fit parameters are the average value μ of the Poisson distribution, the width σ_e of the $n = 0$ peak (also called pedestal) which represents the electronic noise, the width σ_1 of the $n = 1$ peak which is the dispersion of the 1-cell signal.

In Fig. 7 we plot the average value μ as a function of the impinging light intensity, at several bias voltages, for the STM sensor. There is clear evidence of good linear response, and the slight increase in the μ value with increasing bias can likely be interpreted as a slight increase of the Photon Detection Efficiency (PDE) of the sensor. We want to remark here that such a linearity can be expected by a SiPM as long as the fraction of fired cells is small, otherwise the multiple firing effect sets in and plays a non-negligible role [7].

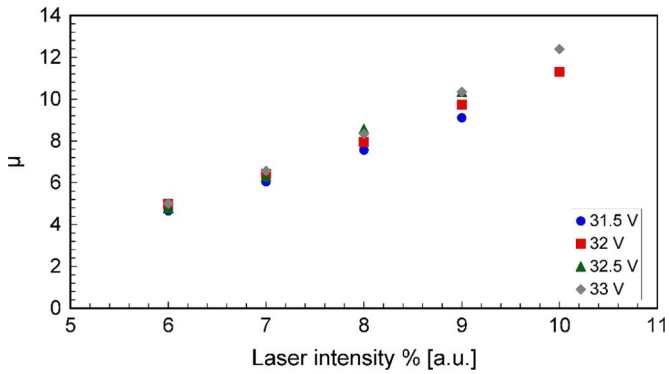

Fig. 7. Average value of the measured Poisson distribution as a function of the light intensity for several values of the bias voltage (STM SiPM).

Fig. 8 shows a different behavior for the Hamamatsu sensor. We observe that at low light intensity we measure a higher value of μ as compared to a linear behavior, and this is consistent with the correlated noise pattern already observed in Figs. 3 and 6.

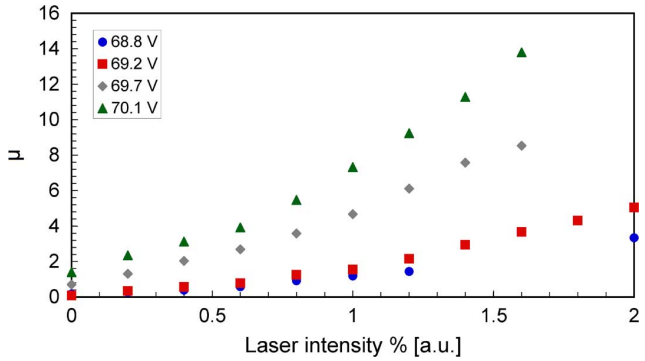

Fig. 8. Average value of the measured Poisson distribution as a function of the light intensity for several values of the bias voltage (Hamamatsu SiPM).

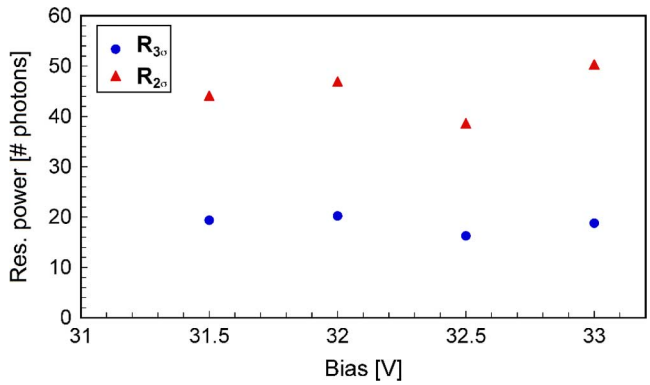

Fig. 9. Resolving power at 3σ and 2σ for the STM SiPM at different bias voltages. The multipeak structure of the charge spectrum will still be clearly resolved around $\mathrm{n} = 20$, and will disappear around $\mathrm{n} = 45$.

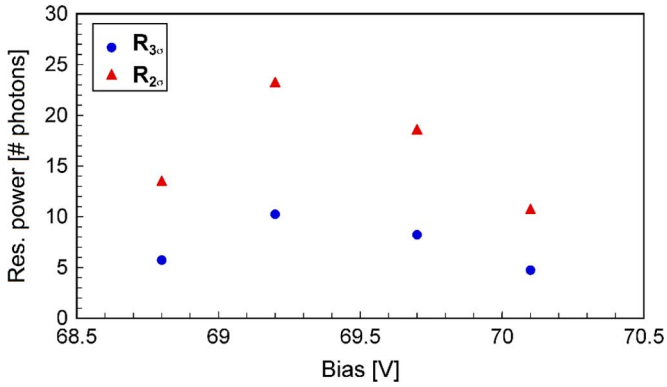

Fig. 10. Resolving power at 3σ and 2σ for the Hamamatsu SiPM at different bias voltages. The multipeak structure of the charge spectrum will still be clearly resolved around $\mathrm{n} = 7$, and will disappear around $\mathrm{n} = 17$.

Moreover, there is a large variation of the μ value with the bias voltage. As such a dramatic change in PDE is unlikely, we attribute this effect to a considerable increase of the correlated noise with the bias voltage.

As to the σ_1 values, for each measurement we normalized it to the centroid of the $n = 1$ peak, in order to be able to compare all the measurements at once. We found that $\sigma_1/c(1)$ has an average value around 11% for the STM device and 18% for the Hamamatsu sensor, with quite a larger spread for the values of the latter.

The values of σ_e and σ_1 allow quick evaluation of the photon resolving power of each device.

According to [27], [33] the resolving power $R_{k\sigma}$ for any chosen k value, is the number n of detected photons where the peak spacing d equals $k\sigma$. In formulas

$$\begin{aligned} d &= k\sigma_{\mathrm{tot}}(n) \\ \sigma_{\mathrm{tot}}^2 &= \sigma_e^2 + n\sigma_1^2 \\ R_{k\sigma} &= \frac{1}{\sigma_1^2}\left(\frac{d^2}{k^2} - \sigma_e^2\right) \end{aligned} \tag{1}$$

In Figs. 9 and 10 we show the resolving power at 3σ and 2σ $(k = 3; 2)$ respectively for the STM and the Hamamatsu sensors. Even though this parameter is sensitive to the bias voltage, we can roughly state that the STM SiPM still resolves discrete photon peaks at $n = \langle R_{3\sigma}\rangle \approx 20$, and its multipeak structure washes out around $n = \langle R_{2\sigma}\rangle \approx 45$. As to the Hamamatsu SiPM we observe $n = \langle R_{3\sigma}\rangle \approx 7$ and $n = \langle R_{2\sigma}\rangle \approx 17$.

In order to show such a resolving power in operation we summed, for each sensor, all of the charge spectra taken at different light intensity with the same bias voltage. This should somehow emulate the detection of a wider range of impinging number of photons. The result for the two sensors is shown in Figs. 11 and 12.

By knowing the average distance between two peaks in terms of QDC (charge to digital converter) channels, transforming it into charge and scaling by the known linear amplifier gain, we could easily calculate the gain for the two devices at each bias voltage, as it represents the number of electrons generated per detected photoelectron [29]. We observed that in both cases the gain scales linearly with the bias voltage, as expected. However, for reasons not well understood the measured gain for the Hamamatsu SiPM keeps roughly a factor 6 below what stated in its datasheet. We checked this on a second sample finding the same result. Therefore we cross checked the gain using a totally different charge-sensitive amplifier, again finding the same factor 6. This matter is worth further investigation.

III. Noise

A. Dark Counts Versus Threshold

Firstly we explored the dark count rate as a function of the threshold, employing a leading edge discriminator followed by a fast digital pulse counter. The measurement results are reported in Figs. 13 and 14. What is immediately evident is that even though the two devices have dark noise of the same order of magnitude at 0.5 ph threshold, the STM device noise is strongly suppressed already at 1.5 ph threshold. The same amount of reduction is not seen for the Hamamatsu sensor even at 3.5 ph threshold. This is a strong indication of the presence of correlated noise, which confirms what could be inferred from Fig. 3.

A rough estimate of such correlated noise can be obtained by computing the ratio between the counting rate at 1.5 ph and 0.5 ph threshold. This ratio comes out about 0.5% for the STM SiPM and 27% for the Hamamatsu SiPM. This is not a surprise, as the STM device features the mentioned opto-insulating trench around each cell that cuts down the optical cross-talk. The cross-talk figure measured for the Hamamatsu is in agreement with the value reported in [6].

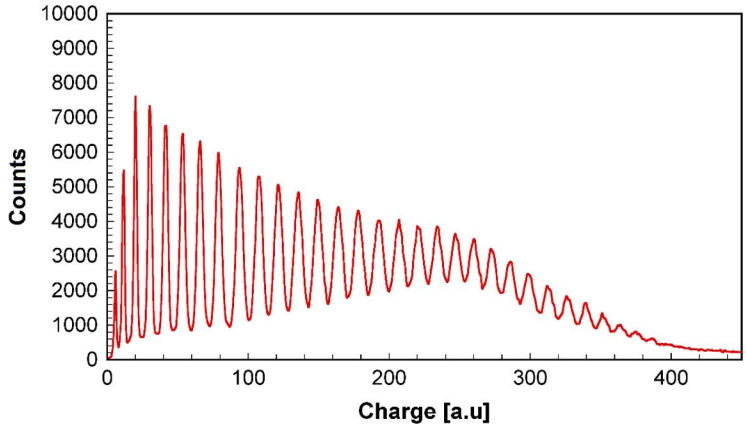

Fig. 11. Sum of several charge spectra taken at different light intensity with 32.5 V bias voltage, in order to emulate the detection of a wider range of impinging number of photons, for the STM SiPM. Peaks are still well resolved at $n = 30$.

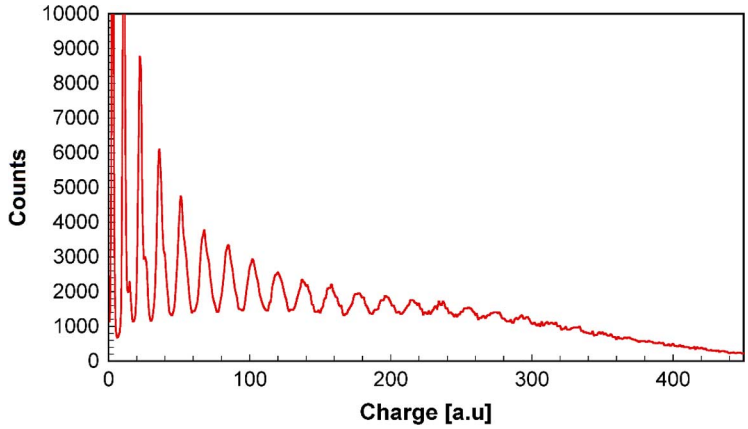

Fig. 12. Sum of several charge spectra taken at different light intensity with 69.7 V bias voltage, in order to emulate the detection of a wider range of impinging number of photons, for the Hamamatsu SiPM. The multipeakpeak structure is washed out at $n = 18$.

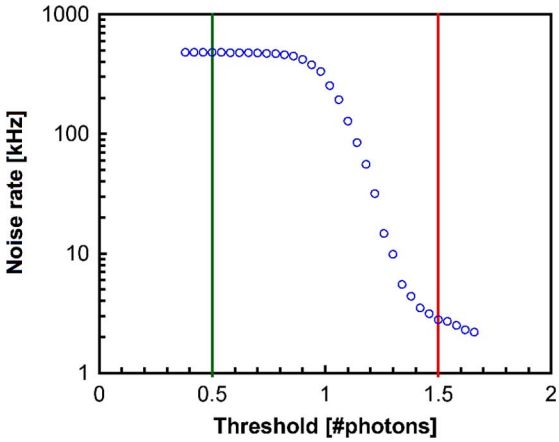

Fig. 13. Dark counting rate versus threshold for the STM SiPM at 32.5 V bias. The noise level at 1.5 ph is tiny, indicating a low level of correlated noise. As a guide to the eye we show the 0.5 ph and 1.5 ph threshold lines.

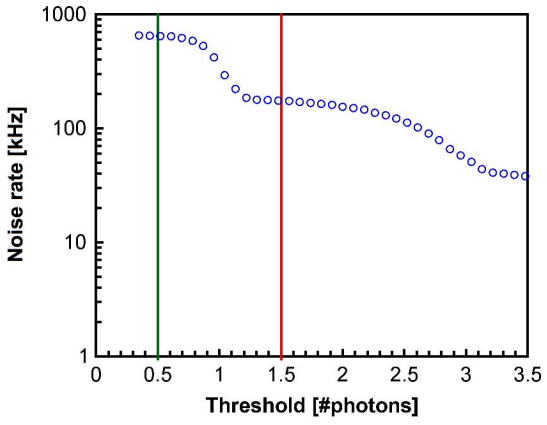

Fig. 14. Dark counting rate versus threshold for the Hamamatsu SiPM at 69.7 V bias. The noise level at 2.5 ph and 3.5 ph is still considerable, confirming a non-negligible correlated noise level as already guessed from Fig. 3. As a guide to the eye we show the 0.5 ph and 1.5 ph threshold lines.

B. Dark Counts Time Distribution

Our second method for the evaluation of the device noise is based on measuring the distribution of the time intervals between two consecutive dark pulses. Therefore we set our threshold at 0.5 ph and set up a Time-to-Amplitude Converter (TAC) system in order to build up a histogram. We do not go into the details of the electronics setup, described in [27], [33]. We did this for each SiPM at all the bias voltages, and found that the two devices have a rather different behavior. We report in Fig. 15 a sample plot of the time distribution for the STM device. What one expects from a Poisson behavior is an

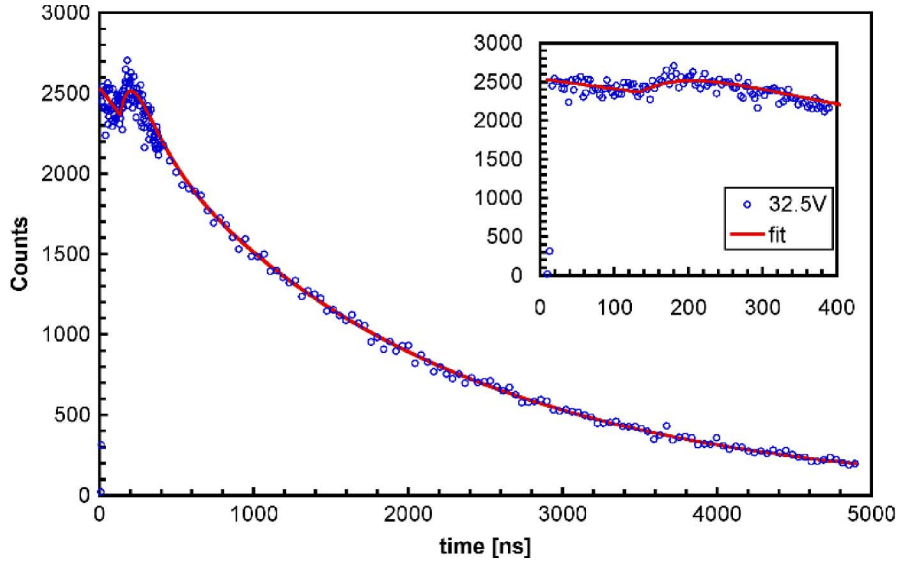

Fig. 15. Distribution of the time interval between two counts for the STM SiPM biased at 32.5 V. The inset is a zoom of the 0–400 ns range. The overall behavior is exponential, according to Poisson's law, with a small bump due to afterpulsing around 200 ns.

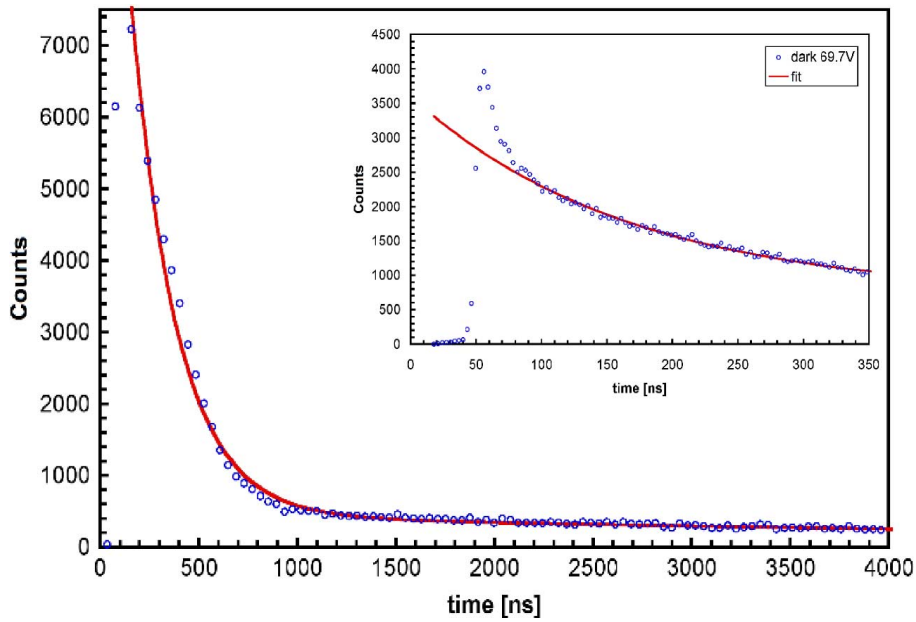

Fig. 16. Distribution of the time interval between two counts for the Hamamatsu SiPM biased at 69.7 V. The inset is a zoom of the 0–350 ns range. At variance with the STM case the plot shows at least three exponential slopes, pointing to a non-random behavior.

exponential function whose slope is the average counting rate. This is exactly what we found, apart from a little bump around 200 ns which we attributed to afterpulsing and fitted under the following assumptions:

- an afterpulse occurring before a given time generates a smaller signal which is below the discriminator threshold and therefore is not detected;
  the afterpulses capable of triggering the discriminator will follow an exponential recharge curve, while the cell is recharging to its bias voltage, and then another exponential discharge slope.

This is indeed what we observe, which is also consistent with the known RC parameters of the device cells.

We remark that by this method, due to the electronic setup, there is an unavoidable dead time of 30 ns below which we cannot observe signals. Therefore this method is not suitable for evaluating cross-talk noise.

We repeated the procedure for the Hamamatsu SiPM. Instead of finding a Poisson behavior with an afterpulsing bump, we found a decreasing function with three exponential slopes. This means that the lower the time interval after a pulse, the higher the probability that a correlated pulse occurs. This behavior is clearly shown in Fig. 16. The main exponential slope is indeed smooth, of the order of 5–20 μs which represents a better noise figure with respect to the 1.6–3 μs of the STM SiPM. Unfortunately on top of this relatively low random noise figure there

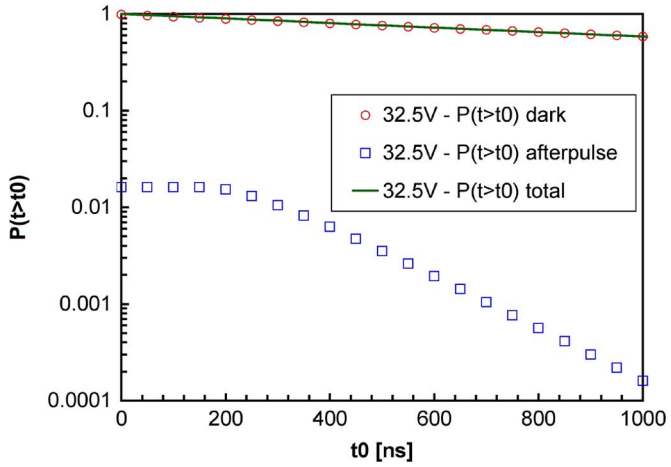

Fig. 17. Probability of a dark pulse to occur after a time t_0 following another pulse, for the STM SiPM biased at 32.5 V (line). The contributions of random counts (circles) and correlated afterpulses (squares) are individually shown. Afterpulsing is negligible after 500 ns.

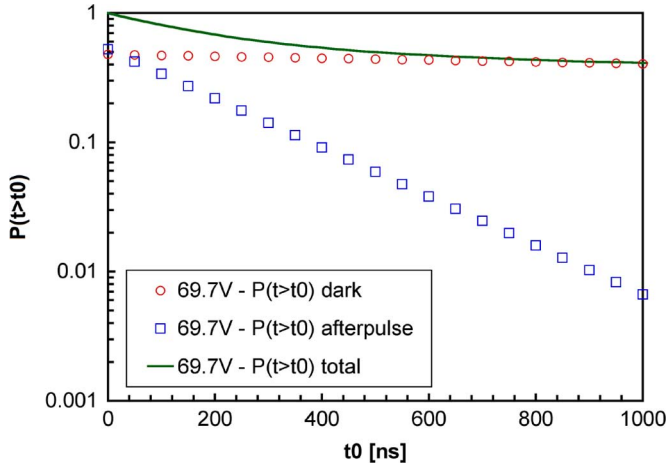

Fig. 18. Probability of a dark pulse to occur after a time t_0 following another pulse, for the Hamamatsu SiPM biased at 69.7 V (line). The contributions of random counts (circles) and correlated afterpulses (squares) are individually shown. Afterpulsing is relevant at least until 800 ns.

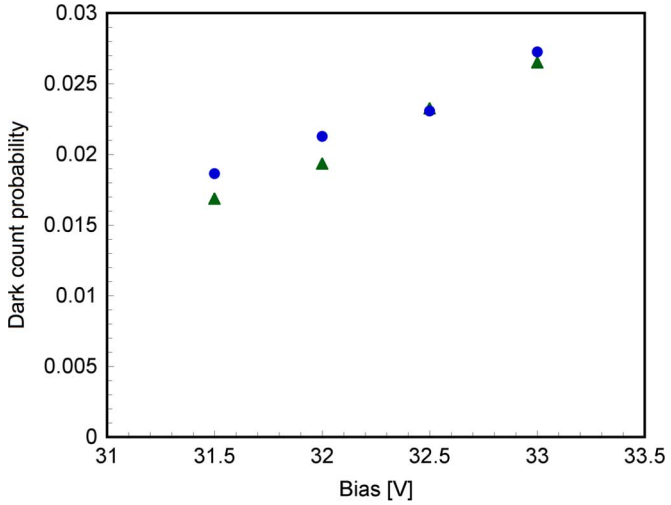

Fig. 19. Probability of two dark pulses to occur within a 30 ns gate for the STM SiPM, as obtained by comparing the areas of the first two peaks in the charge spectrum of the dark noise, at different bias voltage values (circles). Also reported is the expected Poisson behavior as evaluated from the previous fit of Fig. 15 (triangles). The difference between each pair of points is to be ascribed to fast occurring correlated pulses, i.e., cross-talk. See text for further details.

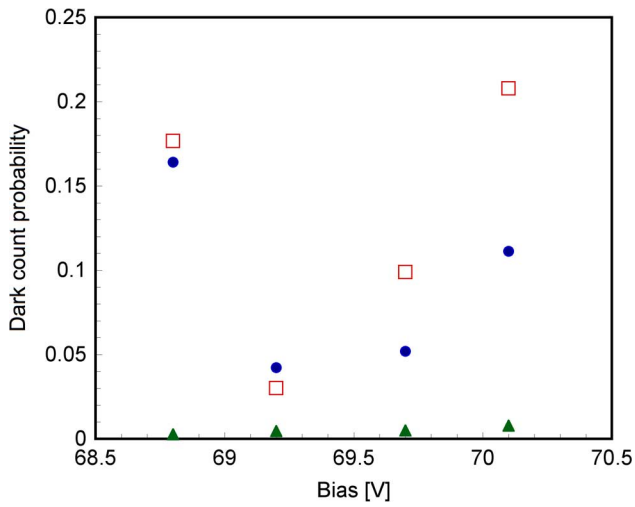

Fig. 20. Probability of two dark pulses to occur within a 30 ns gate for the Hamamatsu SiPM, as obtained by comparing the areas of the first two peaks in the charge spectrum of the dark noise, at different bias voltage values (circles). Also reported is the expected Poisson behavior as evaluated from the previous fit of Fig. 16 (triangles). The difference between each pair of points is to be ascribed to fast occurring correlated pulses, i.e., cross-talk. If the first three peaks are used for this calculation, the cross-talk comes out still higher (squares). See text for the explanation of the points at 68.8 V bias.

is a huge amount of correlated noise with two additional faster exponential slopes of the order of 20 ns and 200 ns.

Using the fit parameters we are able to write down the normalized probability distribution in analytical form, and therefore to integrate it in order to provide the probability of a dark count to occur after a given time t_0. Such a probability is reported in Figs. 17 and 18 for the two devices. We remark that in the analytical expression of this probability, in the case of the Hamamatsu SiPM we did not include the fastest exponential slope. This implies that its real behavior at short time scale is to be expected worse than shown here.

C. Dark Counts Charge Distribution

The third method we employed to evaluate the noise is the charge distribution spectrum of the dark pulses, acquired with a 30 ns integration gate. Even though we do not make any correction for the dead time of the data acquisition system, by comparing the number of events under each peak we can gather information about the statistical behavior of the sensors. Simple mathematics allows us to compute the ratio between two peaks or any combination of peaks, as expected in case of a Poisson distribution. Any deviation from such a behavior is to be ascribed to some correlation in the events.

We integrated the first two peaks of the dark count charge spectrum of each SiPM both by rough graphical cuts and by fitting the peaks with Gaussians, obtaining equivalent results.

In Fig. 19 we plot the Poisson expectation for the ratio between the areas of the first two peaks (triangles) as evaluated from the fit of Fig. 15, at several bias voltage values. We then

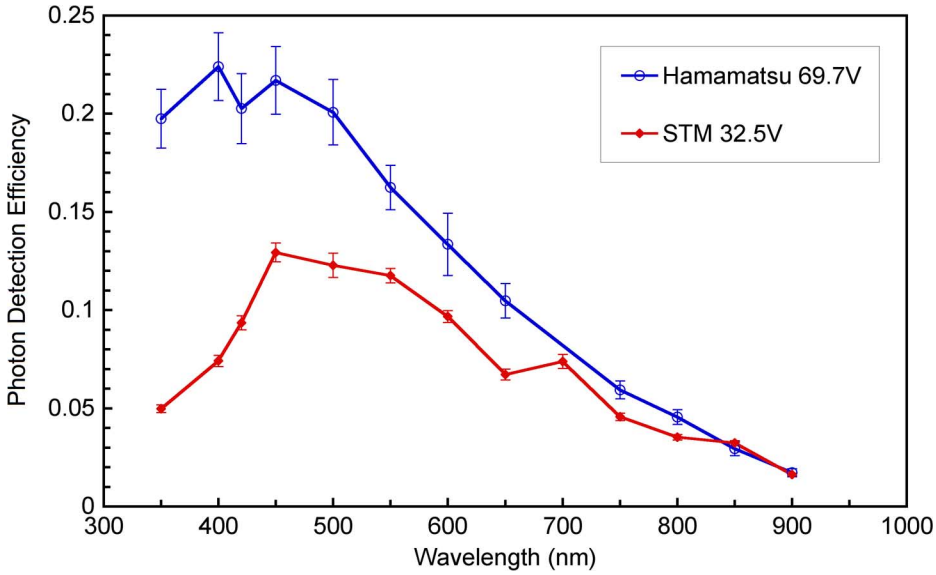

Fig. 21. Photon Detection Efficiency (PDE) for the two photosensors. The better geometrical fill factor for the Hamamatsu SiPM (78%) with respect to the STM SiPM (36%) is quite evident.

report the effectively measured ratio, remarking that the difference between each pair of points is to be ascribed to fast occurring correlated pulses, i.e., cross-talk. We can see that in this case it is of the order of 0.1%.

When building the same plot for the Hamamatsu SiPM, shown in Fig. 20, we immediately see a significant difference between the Poisson behavior and the measured data. Moreover, if we include the first three peaks in the calculation (this is possible because there was a considerable number of counts in the $\mathrm{n} = 3$ peak), we find a still higher deviation from the pure random behavior.

A further prove that by means of this analysis we can detect correlations is given by a mistake we made in our experimental procedure. The dark measurements were done with no fiber on the detector, but at 68.8 V bias we forgot to remove the fiber and only set the nominal laser intensity at 0%. Therefore in this case there was a tiny probability to detect some real correlated photons, and this was highlighted by our analysis procedure as can be easily seen at 68.8 V in Fig. 20.

IV. Photon Detection Efficiency

As for the Photon Detection Efficiency we have discovered that the integral photocurrent measurements described in the literature are likely to be affected by systematic errors induced by noise, cross-talk, afterpulsing [29], as also reported in the datasheet of the Hamamatsu SiPM. Therefore we devised a different approach, based on single photon counting, which we proved to be very effective especially with respect to the suppression of the correlated noise.

Our method, described in detail in [28], makes use of a monochromator, an integrating sphere, and a NIST calibrated reference photodiode. It basically consists of the following steps:

- the threshold is set on the 1-photon plateau (0.5 ph);
- SiPM and reference NIST photodiode are attached to the output port of the integrating sphere;
- the monochromatic light intensity is kept low (no 2-photon events on the SiPM);
- the pulse to the counter is wide enough (holdoff) to reduce the correlated noise to negligible level;
- pulses are counted with and without light, signal counts are obtained by subtraction;
- deadtime correction is applied.

In Fig. 21 we show the PDE for the two photosensors as obtained with our single photon method. We also tested the method by changing the duration of the pulse to the counter (holdoff) and correcting the measurements accordingly. The final result was identical to what shown, thus proving its correctness. We remark that the better geometrical fill factor of the Hamamatsu SiPM is immediately evident from Fig. 21, as well as its better efficiency in the blue wavelength region (350–450 nm).

V. Conclusion

The procedure we established to measure several features of SiPM photodetectors proved to be self consistent, and it allowed us to perform a rather exhaustive comparison between two devices built in different technologies by different manufacturers. Our main remark, after comparing our results with others present in the literature, is that special care needs to be taken in handling the correlated noise of these sensors, namely afterpulses and cross-talk, especially when measuring very low intensity light pulses. As an example, in our current application for the detection of thermal neutrons by means of ^{6}Li screens and scintillating fibers [32], a low level of correlated noise is mandatory: the resolution in the region of few (real) photons is needed to discriminate gamma rays from neutrons, and we could not tolerate the amount of fake photon counts produced by the Hamamatsu sensor.

References

[1] V. D. Kovaltchouk *et al.*, "Comparison of a silicon photomultiplier to a traditional vacuum photomultiplier," *Nucl. Instrum. Meth. A*, vol. 538, pp. 408–415, 2005.

[2] P. Buzhan *et al.*, "Silicon photomultiplier and its possible applications," *Nucl. Instrum. Meth. A*, vol. 504, pp. 48–52, 2003.
[3] V. Golovin and V. Saveliev, "Novel type of avalanche photodetector with Geiger mode operation," *Nucl. Instrum. Meth. A*, vol. 518, pp. 560–564, 2004.
[4] I. Britvitch *et al.*, "Development of scintillation detectors based on avalanche microchannel photodiodes," *Nucl. Instrum. Meth. A*, vol. 571, pp. 317–320, 2007.
[5] I. Britvitch *et al.*, "Investigation of a photon counting avalanche photodiode from Hamamatsu photonics," *Nucl. Instrum. Meth. A*, vol. 567, pp. 276–280, 2006.
[6] S. Gomi *et al.*, "Development and study of the multi pixel photon counter," *Nucl. Instrum. Meth. A*, vol. 581, pp. 427–432, 2007.
[7] D. Renker, "New trends on photodetectors," *Nucl. Instrum. Meth. A*, vol. 571, pp. 1–6, 2007.
[8] A. Heering *et al.*, "Performance of silicon photomultiplers with the CMS HCAL front-end electronics," *Nucl. Instrum. Meth. A*, vol. 576, pp. 341–349, 2007.
[9] H. Gast *et al.*, "A high resolution scintillating fiber tracker with SiPM readout," *Nucl. Instrum. Meth. A*, vol. 581, pp. 423–426, 2007.
[10] G. Collazuol *et al.*, "Single photon timing resolution and detection efficiency of the IRST silicon photo-multipliers," *Nucl. Instrum. Meth. A*, vol. 581, pp. 461–464, 2007.
[11] D. J. Herbert *et al.*, "First results of scintillator readout with silicon photomultiplier," *IEEE Trans. Nucl. Sci.*, vol. 53, no. 1, p. 389, 2006.
[12] P. Buzhan *et al.*, "Large area silicon photomultipliers: Performance and applications," *Nucl. Instrum. Meth. A*, vol. 567, pp. 78–82, 2006.
[13] *SensL SiPMPlus Device for the GlueX Project at Jefferson Lab.*, [Online]. Available: http://www.sensl.com/Products/
[14] D. M. Taylor, J. C. Jackson, A. P. Morrison, A. Mathewson, and J. G. Rarity, "Characterization of novel active area silicon avalanche photodiodes operating in the Geiger mode," *J. Mod. Opt.*, vol. 51, no. 9/10, pp. 1323–1332, 2004.
[15] M. Mazzillo *et al.*, "Single photon avalanche photodiode arrays," *Sens. Actuators A*, vol. 138, pp. 306–312, 2007.
[16] P. Finocchiaro *et al.*, "A new generation of low-voltage single-photon micro-sensors with timing capability," *Nucl. Instrum. Meth. A*, vol. 567, pp. 83–88, 2006.
[17] E. Sciacca *et al.*, "Arrays of geiger mode avalanche photodiodes," *IEEE Photon. Technol. Lett.*, vol. 18, no. 15, pp. 1633–1635, 2006, and references therein.
[18] M. Mazzillo *et al.*, "Single photon avalanche photodiodes with integrated quenching resistor," *Nucl. Instrum. Meth. A*, submitted for publication.
[19] A. C. Giudice *et al.*, "A process and deep evaluation tool: Afterpulsing in avalanche junctions," in *Proc. 33rd Conf. on Eur. Solid-State Device Res.*, 2003, vol. 1, pp. 347–350.
[20] J. C. Jackson *et al.*, "Towards integrated single photon counting microarrays," *Opt. Eng.*, vol. 42, no. 1, pp. 112–118, 2003.
[21] B. Dolgoshein *et al.*, "Status report on silicon photomultiplier development and its applications," *Nucl. Instrum. Meth. A*, vol. 563, pp. 368–376, 2006.
[22] C. Piemonte *et al.*, "Characterization of the first prototypes of silicon photomultiplier fabricated at ITC-irst," *IEEE Trans. Nucl. Sci.*, vol. 54, no. 1, pp. 236–244, 2007.
[23] P. Finocchiaro *et al.*, "Test of scintillator readout with single photon avalanche photodiodes," *IEEE Trans. Nucl. Sci.*, vol. 52, no. 6, pp. 3040–3046, 2005.
[24] C. Piemonte, "A new silicon photomultiplier structure for blue light detection," *Nucl. Instrum. Meth. A*, vol. 568, pp. 224–232, 2006.
[25] M. Belluso *et al.*, "Electro-optical characteristics of the single photon avalanche diode (SPAD)," *Scientific Detectors Astron.*, pp. 461–467, 2005.
[26] P. Finocchiaro *et al.*, "SPAD-arrays and micro-optics: Towards a real single photon spectrometer," *J. Mod. Opt.*, vol. 54, no. 2/3, pp. 199–212, 2007.
[27] P. Finocchiaro *et al.*, "Characterization of a novel 100-channel silicon photomultiplier (Part 1: Noise)," *IEEE Trans. Elec. Dev.*, to be published.
[28] P. Finocchiaro *et al., Single-photon-counting method for measuring the photon detection efficiency of a silicon photomultiplier*, in preparation.
[29] G. Bonanno *et al.*, Nucl. Instrum. and Meth. A talk given at NDIP 2008, Aix Les Bains, France, to appear on.
[30] *STMicroelectronics, Stradale Primosole*, [Online]. Available: www.st.com, Catania, Italy
[31] *Hamamatsu Photonics*, [Online]. Available: www.hamamatsu.com
[32] P. Finocchiaro *et al.*, "Detector mesh for nuclear repositories," presented at the 11th Topical Seminar on Innovative Particle and Radiation Detectors (IPRD08) Siena.
[33] P. Finocchiaro *et al.*, "Characterization of a novel 100-channel silicon photomultiplier (Part 2: Charge and time)," *IEEE Trans. Elec. Dev.*, to be published.